NEUROSCIENCE

Regulation of energy rheostasis by the melanocortin-3 receptor

Masoud Ghamari-Langroudi[1]*, Isin Cakir[1,2], Rachel N. Lippert[1,3], Patrick Sweeney[2], Michael J. Litt[1], Kate L. J. Ellacott[1,4], Roger D. Cone[1,2]*

Like most homeostatic systems, adiposity in mammals is defended between upper and lower boundary conditions. While leptin and melanocortin-4 receptor (MC4R) signaling are required for defending energy set point, mechanisms controlling upper and lower homeostatic boundaries are less well understood. In contrast to the MC4R, deletion of the MC3R does not produce measurable hyperphagia or hypometabolism under normal conditions. However, we demonstrate that MC3R is required bidirectionally for controlling responses to external homeostatic challenges, such as caloric restriction or calorie-rich diet. MC3R is also required for regulated excursion from set point, or rheostasis, during pregnancy. Further, we demonstrate a molecular mechanism: MC3R provides regulatory inputs to melanocortin signaling, acting presynaptically on agouti-related protein neurons to regulate γ-aminobutyric acid release onto anorexigenic MC4R neurons, exerting boundary control on the activity of MC4R neurons. Thus, the MC3R is a critical regulator of boundary controls on melanocortin signaling, providing rheostatic control on energy storage.

INTRODUCTION

Adipose stores in mammals are tightly regulated and defended during nutritional challenges, indicating existence of a mechanism that maintains energy stores near a set point. The molecular mechanisms underlying the control of energy stores between upper and lower homeostatic boundaries are incompletely understood. The crucial role of the melanocortin-4 receptor (MC4R) neuronal pathway in regulating energy homeostasis was established both pharmacologically (*1*) and genetically (*2*). MC4R homozygous and heterozygous knockout (KO) mice (*2*), as well as humans (*3*), present with early onset severe obesity associated with hyperphagia, reduced autonomic outflow and energy expenditure (EE), and significantly reduced response to the adipostatic hormone leptin. Hence, the MC4R acts at the heart of the adipostat, regulating both energy intake and expenditure, and is essential for establishing energy set point. In contrast, disruption of the MC3R produces no measurable hyperphagia or hypometabolism in mice or rats under normal conditions (*4*–*6*). MC3R is primarily expressed in the brain in a relatively small set of nuclei that are largely nonoverlapping with expression of the MC4R (*7*, *8*), a critical site being the proopiomelanocortin (POMC) and agouti-related protein (AgRP) neurons of the arcuate nucleus (*9*, *10*).

While mild late-onset obesity is observed in the MC3R KO mouse and rat, there are seemingly conflicting physiological findings, such as a striking increase in susceptibility to weight loss in experimental models of cachexia in the MC3R KO mouse (*11*, *12*). This is in stark contrast to the MC4R KO mouse, which is protected from anorexia and weight loss relative to wild-type (WT) animals in numerous cachexia paradigms (*11*–*14*). A second observation is that MC3R KO mice exhibit defective responses to fasting or food restriction (*15*) and exhibit defective food anticipatory activity (*16*), suggesting a defect in the function of the orexigenic AgRP neurons in MC3R KO. Further, reduced activation of AgRP and neuropeptide Y (NPY) gene expression during fasting was demonstrated in these models (*15*, *17*). Finally, attempts at selective activation of the MC3R using a moderately MC3R-selective agonist, D-Trp^8-γ-MSH, also produced paradoxical findings in both mice (*18*) and rats (*19*): stimulation of food intake. To better understand the role of the MC3R in the regulation of feeding behavior and energy homeostasis, we have examined the control of feeding, energy accumulation, and EE in MC3R KO versus WT mice in response to a variety of orexigenic and anorexigenic challenges. To build a model of the molecular basis for the role of MC3R in response to these stressors, we have used slice electrophysiology to determine the actions of MC3R on downstream paraventricular nucleus of the hypothalamus (PVN) MC4R target neurons, as this circuit is critical for the regulation of feeding and energy homeostasis (*20*).

RESULTS

Physiological responses to nutritional state affected by loss of the MC3R

As demonstrated previously, MC3R KO mice showed normal ad libitum feeding that was not significantly different from WT mice when monitored at 6, 12, and 24 hours after the beginning of a dark phase (*4*, *5*), while we also observed the hyperphagia resulting from deletion of the MC4R (Fig. 1A). A defect in 24-hour refeeding was seen in the MC3R KO mouse (Fig. 1B), as reported previously (*15*); the reduced food intake persisted for up to 5 days (Fig. 1C), and cumulative food intake did not return to WT levels until 10 days after a 36-hour fast (Fig. 1D).

We next examined the effects of caloric restriction (CR) on body weight in the MC3R KO mouse. Animals were calorie restricted to 70% of their own average daily ad libitum energy intake for a period of time until the lean WT mice lost 30% of their original body weight (~25 days). MC3R KO mice lost significantly more of their body weight during the same period (~36%), showing that MC3R KO mice

[1]Department of Molecular Physiology and Biophysics, Vanderbilt University School of Medicine, 702 Light Hall, Nashville, TN 37232, USA. [2]Life Sciences Institute and Department of Molecular and Integrative Physiology, University of Michigan, 210 Washtenaw Avenue, Ann Arbor, MI 48109–2216, USA. [3]Max Planck Institute for Metabolism Research, Gleueler Strasse 50, 50931 Cologne, Germany. [4]University of Exeter Medical School, Exeter, UK.
*Corresponding author. Email: masoud.ghamari-langroudi@vanderbilt.edu (M.G.-L.); rcone@umich.edu (R.D.C.)

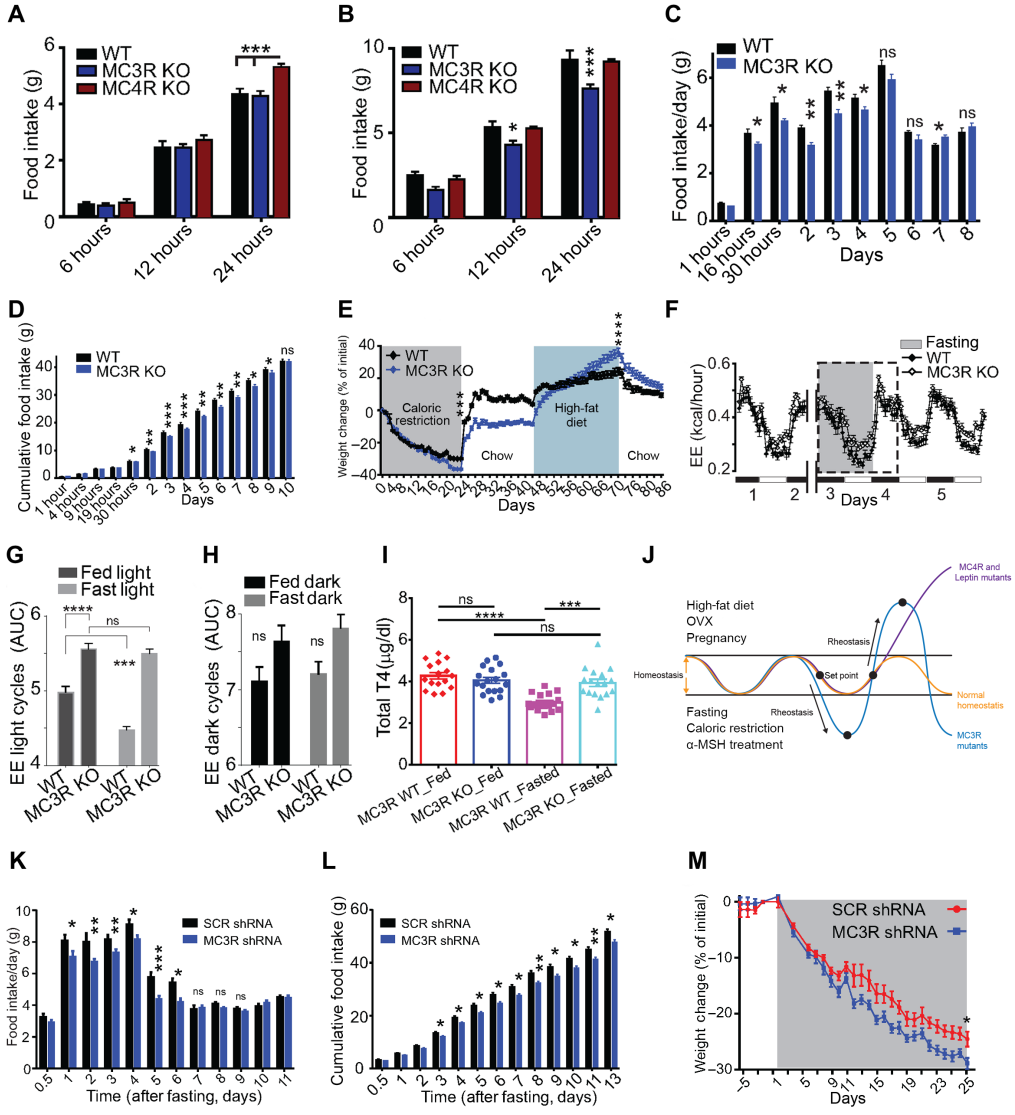

Fig. 1. Dysregulation of responses to both underfeeding and overfeeding following global deletion or viral knockdown of arcuate nucleus MC3R. (**A**) We measured ad libitum food intake of C57BL/6J WT, MC3R KO, and MC4R KO mice on normal chow at 6, 12, and 24 hours, following lights off. In contrast to hyperphagia shown by MC4R KO mice ($n = 6$), MC3R KO ($n = 13$) showed normal feeding compared to WT [$n = 12$; two-way analysis of variance (ANOVA) and Tukey's multiple comparisons test). (**B**) Time course of refeeding after a 24-hour fast. MC3R KO mice ate significantly less compared to WT or MC4R KO mice at 12 and 24 hours of refeeding (two-way ANOVA and Tukey's multiple comparisons test). (**C**) Kinetics of daily food intake after a 36-hour fast. Daily food intake was suppressed in MC3R KO mice from hour 16 to day 4 of refeeding (WT, $n = 12$; MC3R KO, $n = 13$; two-way ANOVA and Sidak's multiple comparisons test). ns, not significant. (**D**) Cumulative food intake in the same cohort, showing a deficit in energy homeostasis sustained for up to 9 days (two-way ANOVA and Sidak's multiple comparisons test). (**E**) Average body weight changes (means and SEM) of MC3R KO ($n = 12$) and WT ($n = 11$) mice in response to CR (gray), followed by ad libitum chow (white), HFD (blue), and then ad libitum chow (white). MC3R KO mice lost significantly more weight than WT mice during CR ($P < 0.001$) and gained more than WT mice on HFD ($P < 0.0001$; two-way ANOVA and Tukey's multiple comparisons test). (**F**) Indirect calorimetry measuring EE of WT and MC3R KO mice in control conditions, in response to a 24-hour period of fasting (shaded area) and to injection of saline, followed by ad libitum refeeding beginning with a dark cycle. (**G**) MC3R KO mice had significantly higher EE than WT animals during the light cycle in both fed and fasted states (Sidak's multiple comparisons test). In contrast to WT mice, MC3R KO mice failed to suppress EE in response to fasting ($P > 0.05$; two-way ANOVA and Tukey's multiple comparisons test). (**H**) The EE of MC3R KO was not different than WT mice during the dark cycle in any metabolic state ($P > 0.05$; Sidak's multiple comparisons test). (**I**) Serum TT4 of MC3R KO ($n = 17$) and WT ($n = 18$) mice in basal fed state and after fasting for 36 hours. The serum TT4 is not significantly different in MC4R KO and WT mice in basal fed states (WT, 4.28 ± 0.16 μg/dl; KO, 4.1 ± 0.15 μg/dl; $P < 0.5$). Fasting fails to cause suppression of the TT4 levels in MC3R KO mice (4.1 ± 0.15 μg/dl in fed to 3.9 ± 0.17 μg/dl during fasting; $P > 0.05$), as opposed to WT mice (4.28 ± 0.16 μg/dl in fed to 3.0 ± 0.09 μg/dl in fasting). The serum TT4 levels in MC3R KO fasted mice was significantly higher than in WT fasted mice (WT fasted mice, 3.0 ± 0.09; KO fasted mice, 3.9 ± 0.17 μg/dl; two-way ANOVA and Tukey's multiple comparisons test). (**J**) MC4R and leptin mutations disrupt maintenance of homeostatic set point, while MC3R mutations disrupt maintenance of upper and lower homeostatic boundary conditions. OVX, ovariectomy. (**K** and **L**) Daily and cumulative food intake after a 36-hour fast observed in mice receiving bilateral arcuate injections of lentivirus expressing shRNA against MC3R ($n = 10$) or control ($n = 9$) scrambled shRNA sequence. Daily food intake in MC3R shRNA–injected mice was significantly less from day 1 up to day 6 of the refeeding period (two-way ANOVA and Tukey's multiple comparisons test). MC3R shRNA–expressing mice failed to compensate for the energy deficit up to 13 days of refeeding (two-way ANOVA). (**M**) Average body weight changes (means ± SEM) of lentivirus-injected mice expressing shRNA against MC3R ($n = 10$) or control scrambled RNA sequence ($n = 9$) in response to 70% calorie restriction. At day 25, MC3R shRNA–expressing mice lost about 30% (29.6 ± 0.98%) of their body weight, significantly lower than scramble shRNA–expressing mice losing 24% of their body weight during the same period ($P < 0.05$ from days 20 to 25; multiple t test). Convention used throughout: ****$P < 0.0001$, ***$P < 0.001$, **$P < 0.01$, *$P < 0.05$.

are unable to appropriately conserve energy when subjected to calorie restriction (Fig. 1E).

Upon termination of CR, we allowed mice ad libitum access to chow and observed an initial rapid weight gain. After 1 week, WT and MC3R KO mice reached new steady-state body weights, suggesting the achievement of an energy set point. However, while the WT lean mice maintained their body weight slightly above their pre-CR values (+3.69 ± 0.82%), MC3R KO mice reached a new steady-state body weight significantly less than their pre-CR values (−8.53 ± 0.88%). After their body weights were stabilized, we then fed the WT lean and MC3R KO mice a high-fat diet (HFD) (60% kcal fat; Research Diets) for a period of 30 days. Data show that WT lean mice reached a new body weight 16% higher than their pre-HFD weight. In contrast, MC3R KO mice gained weight at a much faster rate, reaching a point 29% higher than their initial body weight (Fig. 1E). When the diet was again switched back to regular chow, both groups of mice lost some of the weight they gained during HFD feeding. However, the weight loss was significantly more pronounced for MC3R KO mice (~22%) compared to WT lean mice (~15% of peak body weight). Thus, MC3R KO mice exceed the normal boundaries of weight loss during CR, defend a reduced set point on chow refeeding, and exceed the normal boundaries of regain compared with WT mice when given energy-rich chow.

Since MC3R KO mice fed with equal calories lost more weight than WT littermates during CR, we hypothesized that they must have higher EE than matched WT mice. To test this hypothesis, we individually housed WT and MC3R KO mice, which were matched for lean mass, in indirect calorimetry chambers (Fig. 1F). During the light cycle, we observed that EE was slightly higher in MC3R KO mice compared to WT mice in the fed state [area under the curve (AUC), 4.97 ± 0.08 (WT) versus 5.56 ± 0.079 (MC3R KO); Fig. 1G]; no significant effects were seen in the dark cycle (Fig. 1H). EE in WT mice was suppressed during fasting, but no effect of fasting on EE was observed in MC3R KO mice (Fig. 1G). EE in mammals is suppressed during fasting in part through suppression of the hypothalamic-pituitary-thyroid (HPT) axis (*21*). To address a possible role of thyrotropin-releasing hormone PVN neurons, known to express MC4R (*22*), in dysregulation of the HPT axis, we also measured serum levels of thyroid hormone [total T4 (TT4)] in response to 36 hours of fasting in WT and MC3R KO mice (Fig. 1I). TT4 was not significantly different in MC3R KO and WT mice in basal fed states (WT, 4.28 ± 0.16 μg/dl; KO, 4.1 ± 0.15 μg/dl). As expected, fasting caused significant suppression of the TT4 levels in WT mice (3.0 ± 0.09 μg/dl). However, fasting failed to cause suppression of the TT4 levels in MC3R KO mice (3.9 ± 0.17 μg/dl). The EE and TT4 findings collectively indicate dysregulation of EE in response to nutritional challenges in MC3R KO mice, which is in parallel to defects shown above in the control of feeding. These defects in food intake and EE can explain changes in body weight (Fig. 1E) and point to a defect in constraining both weight loss and weight gain upon loss of the MC3R. Thus, the MC3R does not appear necessary for maintenance of set point per se but for regulation of the upper and lower boundaries of set point, suggesting a role in rheostasis or the regulated movement of set point (Fig. 1J).

MC3R is expressed in multiple brain nuclei (*8*) but is known to be expressed in the melanocortin circuits proper—the AgRP and POMC neurons found in the arcuate nucleus of the hypothalamus (ARC) (*9*). To test the role of the MC3R specifically in the ARC in the phenotypes described here, we knocked down MC3R gene expression by bilateral ARC-specific injection of lentivirus expressing short hairpin RNA (shRNA) against this gene or a scrambled control sequence into C57BL/6J mice. We validated the effectiveness of the virus in knocking down MC3R mRNA in human embryonic kidney (HEK) 293 cells transfected with an MC3R expression vector (fig. S1A) and the efficacy of the viral injections into the ARC by post hoc analysis of viral green fluorescent protein (GFP) expression in ARC and an adjacent uninjected site (fig. S1, B and C). We then conducted postfast refeeding studies as in Fig. 1 (C and D) in these animals. Mice injected with lentiviral particles expressing shRNA against MC3R were unable to refeed as efficiently as mice injected with control virus for up to 7 days after ad libitum refeeding began (Fig. 1K). MC3R shRNA–expressing mice failed to compensate for the energy deficit for up to 13 days of refeeding (Fig. 1L). Furthermore, upon 70% calorie restriction as described previously (Fig. 1E), MC3R shRNA–expressing mice lost about 30% (29.6 ± 0.98%) of their body weight compared to control shRNA–injected mice that lost about 24% of their body weight during the same period (Fig. 1M). These data support a role of MC3R specifically expressed in ARC neurons in mediating the homeostatic responses shown here.

MC3R regulates miniature inhibitory postsynaptic currents in PVN MC4R neurons

We used slice electrophysiology to probe the role of the MC3R in the function of these circuits. We previously characterized effects of α-MSH (alpha-melanocyte-stimulating hormone) and AgRP on various parameters of cellular excitability, such as membrane potential and the intracellular signaling pathways involving postsynaptic MC4R in PVN neurons (*23*–*25*). In addition to these effects on postsynaptic membrane current, we noted that applications of melanocortins such as α-MSH can also increase the synaptic activity in PVN MC4R neurons, suggesting a potential effect involving presynaptic melanocortin receptors, perhaps including MC3R.

We thus sought to examine whether α-MSH modulates the frequency or amplitude of action potential–independent, tetrodotoxin (TTX)–resistant miniature inhibitory postsynaptic currents (mIPSCs) recorded from MC4R-expressing PVN neurons in acute hypothalamic slices (*26*). We performed whole-cell recordings by using CsCl-filled patch electrodes from voltage-clamped neurons held at −70 mV to examine effects of α-MSH on the frequency and amplitude of mIPSCs in brain slices pretreated with TTX, AP5 (D,L-2-amino-5-phosphonopentanoic acid), and NBQX (2,3-dihydroxy-6-nitro-7-sulfamoylbenzo[*f*]quinoxaline), the blockers of fast Na^+ channels, AMPA and NMDA (*N*-methyl-D-aspartate) receptors, respectively. After recording baseline activity, α-MSH was bath-applied for 8 to 13 min and then washed out by switching to control solution (for example, Fig. 2A). We then measured and compared the frequency and amplitude of mIPSCs recorded in control solution, with α-MSH in the bath and after washout. Results showed that α-MSH significantly and reversibly increased the mean frequency (from 3.2 ± 0.42 Hz in control to 4.8 ± 0.6 Hz in peptide; Fig. 2, A to C), but not the amplitude (Fig. 2D), of mIPSCs in MC4R PVN neurons compared to control or wash. The cumulative probability distribution of the frequency [interevent intervals (IEIs)] of mIPSCs was also significantly different in α-MSH compared to control condition (IEI; from 336.0 ± 6.0 ms in control to 185.4 ± 2.2 ms in peptide; Fig. 2E). α-MSH failed to affect the mean or the cumulative probability distribution of the peak amplitude of mIPSCs when compared to control (Fig. 2F). We observed no effect of α-MSH on

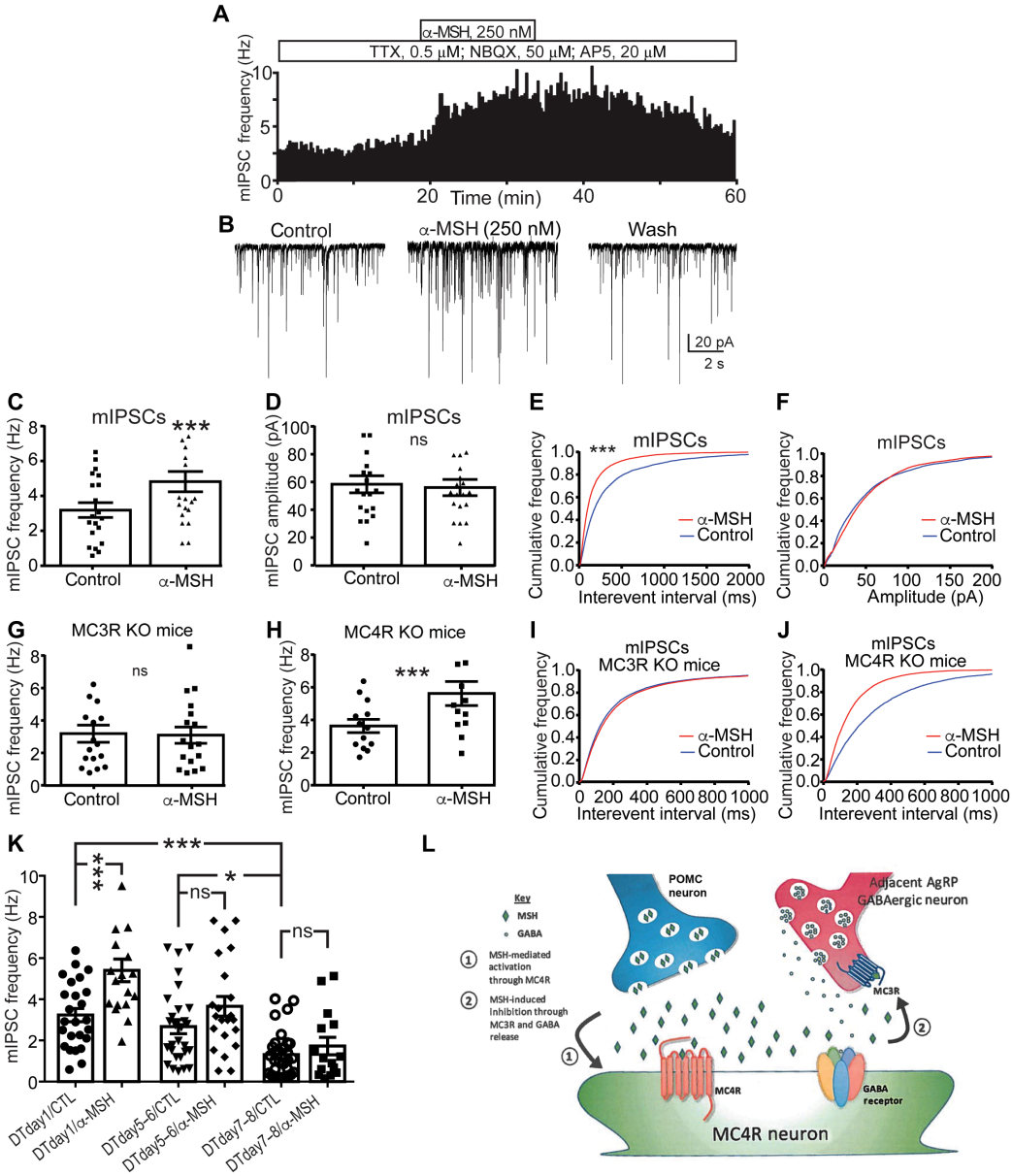

Fig. 2. MC3R signaling in presynaptic AgRP neurons modulates the activity of postsynaptic MC4R PVN neurons through regulation of GABA release. (**A**) Frequency histogram of effects of bath application of 250 nM α-MSH on mIPSCs recorded using CsCl patch electrodes from PVN MC4R neurons held at −70 mV in the presence of 0.5 μM TTX, 25 μM AP5, and 20 μM NBQX to block Na^+-dependent action potential, AMPA, and NMDA receptors, respectively. (**B**) Representative current traces of the same recording in control, α-MSH, and washout. Note the increase in the frequency of mIPSCs in the presence of 250 nM α-MSH, reversible upon washout. (**C** and **D**) The bar graphs represent the means ± SEM of the frequency or amplitude of mIPSCs in control and in 250 nM α-MSH. The peptide significantly increases the mean frequency of mIPSCs (from 3.2 ± 0.42 Hz in control to 4.8 ± 0.58 Hz in peptide; paired *t* test; $n = 20$). The peptide has no significant effect on the mean amplitude of mIPSCs (from 58.36 ± 6.2 pA in control to 56.0 ± 5.80 pA in peptide; ns indicates $P > 0.05$, by paired *t* test; $n = 19$). (**E** and **F**) Cumulative frequency distribution of the frequency or amplitude of mIPSCs (IEI; from 336.0 ± 6.0 ms in control to 185.4 ± 2.2 ms in peptide; Kolmogorov-Smirnov test). (**G** and **H**) Bar graphs indicate the means ± SEM of the frequency of mIPSCs recorded from PVN MC4R neurons from MC3R KO (G) or MC4R KO (H) mice in control and 250 nM α-MSH (from 3.63 ± 0.41 Hz in control to 5.62 ± 0.73 Hz in α-MSH; paired *t* test; $n = 13$). (**I** and **J**) Cumulative frequency distribution of the mIPSC frequency response to α-MSH in tissue from MC3R KO (I) and MC4R KO (J) mice (by Kolmogorov-Smirnov test). (**K**) Bar graphs (means ± SEM) indicate basal frequency of mIPSC after control (CTL) or α-MSH treatment on day 1 (CTL, 3.2 ± 0.32 Hz; $n = 23$), days 5 and 6 (CTL, 2.67 ± 0.34 Hz; $n = 15$), and days 7 and 8 (CTL, 1.3 ± 0.2 Hz; $n = 21$) after intraperitoneal injection of DT into AgRP DTR × MC4R-GFP mice. We administered DT in the morning on days 0 and 2 and prepared sections for electrophysiological analyses on the mornings of the days indicated (two-way ANOVA and Tukey's multiple comparisons test; $^{***}P < 0.001$, $^{*}P < 0.05$, ns indicates $P > 0.05$).

the presynaptic release of glutamate onto MC4R neurons, which was determined by recording frequency and amplitude of excitatory postsynaptic currents (EPSCs; fig. S2).

It is possible that α-MSH acting on postsynaptic MC4R neurons causes the release of retrograde neurotransmitters that act on presynaptic sites to increase γ-aminobutyric acid (GABA) release. Since both endocannabinoids and nitric oxide are known to function as retrograde neurotransmitters, we pretreated brain slices with and included in the external recording solution either 10 μM AM251, a cannabinoid type 1 receptor blocker, or 100 μM L-NAME (NG-nitro-L-arginine methyl ester), a nitric oxide synthase inhibitor. These treatments failed to affect the basal frequency of mIPSCs recorded from MC4R PVN neurons or the α-MSH–induced increase in frequency of mIPSCs (fig. S3).

MC3R mRNA is expressed in ARC AgRP/NPY neurons (*9*), and data suggested that MC3R may regulate release of GABA from AgRP terminals synapsing onto POMC neurons (*27*). We thus tested whether the α-MSH–induced increase in the frequency of mIPSCs in MC4R PVN neurons required MC3R by generating MC4R-GFP × MC3R KO and MC4R-GFP × MC4R KO mice. We then examined effects of α-MSH on the frequency and amplitude of mIPSCs recorded from PVN MC4R neurons in these mice. α-MSH failed to increase the mean and cumulative probability distribution of mIPSC frequency (Fig. 2, G and I) recorded from MC3R KO mice but did so in MC4R KO mice (Fig. 2, H and J), demonstrating the role of the MC3R in this phenomenon.

Since AgRP neurons are GABAergic, we investigated effects of deletion of AgRP neurons on GABAergic inputs recorded from PVN neurons. By crossing MC4R-GFP to mice expressing the diphtheria toxin (DT) receptor (DTR) under the control of the AgRP promoter (*28*), we generated MC4R-GFP mice that express DTR selectively in AgRP neurons. We then treated mice with two intraperitoneal injections of DT (50 μg/kg, at day 0 and day 2), resulting in a significant reduction in ARC AgRP neuron numbers (fig. S4). As reported previously, deletion of AgRP neurons by DT injections causes anorexia and weight loss. We then measured and compared the frequency of mIPSCs at day 1, days 5 and 6, and days 7 and 8 after injections (Fig. 2K). The average basal frequency of mIPSCs recorded from PVN MC4R neurons in control condition was significantly diminished by deletion of AgRP neurons. The mIPSC frequency recorded at days 7 and 8 (mean ± SEM, 1.3 ± 0.2 Hz), when mice have lost about 25 to 30% of their original body weight, was significantly smaller than at day 1 (3.24 ± 0.32 Hz) or than at days 5 and 6 after injection (2.67 ± 0.34 Hz). Furthermore, although α-MSH significantly increases the mIPSC frequency in day 1 (from 3.24 ± 0.32Hz in control to 5.40 ± 0.55 Hz in peptide), this peptide fails to affect the frequency of these events when tested at days 5 and 6 (from 2.67 ± 0.34 Hz in control to 3.66 ± 0.48 Hz in peptide) or days 7 and 8 (from 1.31 ± 0.20 Hz in control to 1.73 ± 0.42 Hz in peptide). At least half of the basal inhibitory activity recorded from PVN neurons thus appears to originate from AgRP neurons in ARC; all of the α-MSH–inducible increase in IPSC frequency appears to require intact AgRP neurons. These data demonstrate that presynaptic MC3R in AgRP neurons exert inhibitory feedback on the POMC-MC4R circuit by regulation of GABA release onto MC4R neurons (Fig. 2L).

MC3R modulates the in vivo response to anorexigenic melanocortin agonists

Since slice electrophysiology demonstrated a role for MC3R in regulating PVN MC4R neurons, we next sought to examine the regulation of MC4R-mediated responses in vivo in the presence and absence of the MC3R, following exogenous administration of an α-MSH analog. We chose a stable and potent peptide analog of α-MSH, LY2112688, as this peptide is a full agonist of MC3R and MC4R and can produce MC4R-dependent inhibition of food intake following peripheral administration (*29*). Following a 24-hour fast, mice were injected intraperitoneally (ip) with vehicle or LY2112688 (10 mg/kg) and given chow ad libitum, 30 min before the onset of the dark phase. We then measured food intake at 1, 4, 12, 18, and 24 hours (Fig. 3A). LY2112688 caused comparable suppression of food intake in both MC3R KO and WT mice at 1 hour of feeding compared to vehicle ($P < 0.05$). However, the LY2112688-induced inhibition of food intake was significantly greater in MC3R KO mice than in WT mice at all time points measured after 1 hour. Thus, much as MC3R KO mice exhibited lack of appropriate responses to the orexigenic stimulus of a fast, they also exhibited a prolonged response to the anorexigenic stimulus of administration of an α-MSH analog, thus demonstrating defective restraint of MC4R-mediated

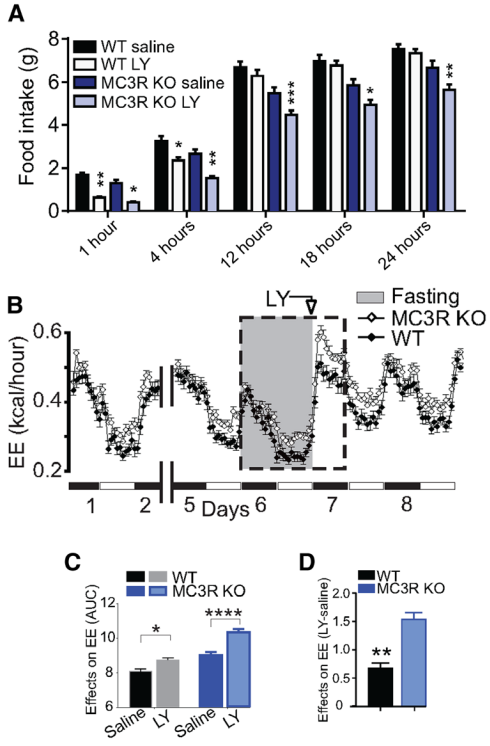

Fig. 3. In vivo evidence of dysregulation of MC4R neuronal activity in the absence of the MC3R. (**A**) Effects of α-MSH analog LY2112688 (LY; 10 mg/kg) on food intake in WT and MC3R KO mice following a 24-hour fast. Bar graphs indicate means ± SEM. Note that LY2112688 caused comparable suppression of food intake in both MC3R KO and WT mice at 1 and 4 hours after refeeding. The effects of LY2112688 disappear in WT mice at later time points but persist at all the time points up 24 hours in MC3R KO mice ($n = 12$ per group; two-way ANOVA and Tukey's multiple comparisons test). (**B**) Recording of indirect calorimetry demonstrates EE of WT and MC3R KO mice in control conditions, in response to a 24-hour period of fasting (shaded areas) and to injection of LY2112688 (10 mg/kg), followed by ad libitum refeeding beginning with a dark cycle. (**C**) The AUC of EE responses of mice to saline and LY2112688 indicates that LY2112688 causes a heightened thermogenic response in MC3R KO compared to WT mice (two-way ANOVA and Tukey's multiple comparisons test). (**D**) AUC of LY211063-induced EE response in WT and MC3R KO mice [in (B) to (D); $n = 20$ male mice; ****$P < 0.0001$, ***$P < 0.001$, **$P < 0.01$, *$P < 0.05$, two-way ANOVA and Tukey's multiple comparisons test].

anorexigenic activity in vivo in the absence of the MC3R. LY2112688 caused an increase in EE compared to saline in WT and MC3R KO mice, which were matched for lean mass (Fig. 3, B and C). However, the LY2112688-induced increase in EE was almost 3× greater in MC3R KO mice than in WT animals (Fig. 3D), also suggesting defective restraint of MC4R effects on EE.

Reproductive state alters physiological responses in the MC3R KO mouse

Changes in reproductive state also represent an internal challenge to the maintenance of energy stores. For example, the increased energy demands of pregnancy result in significant changes in energy intake and storage; this regulated escape from established to new homeostatic set points is referred to as rheostasis (*30*). Mice are known to exhibit a ~50% increase in daily food intake during pregnancy, and thus, WT and MC3R KO pregnant mice were analyzed for food intake and body weight changes during gestation. MC3R KO female animals showed a significant blunting of daily food intake (Fig. 4A) during the middle stage of pregnancy, between days 7 and 12 (Fig. 4B). Analysis of the entire pregnancy shows a sustained reduction in cumulative food intake (Fig. 4C). When compared to nonpregnant-matched genotype controls, both WT and MC3R KO animals showed a significant increase in food intake during pregnancy (Fig. 4D); however, MC3R KO animals showed a blunted increase in food intake in comparison to WT pregnant controls (Fig. 4D). This alteration in food intake does not elicit a detectable difference in total body weight change throughout pregnancy between genotypes (Fig. 4E); however, when adipose mass is carefully measured near the end of pregnancy, WT animals exhibit an increase in fat mass, while no pregnancy-induced increase in adipose mass is seen in the MC3RKO (Fig. 4F). Another rheostatic increase in energy stores associated with reproductive state often occurs during menopause. Modeling this using ovariectomy in the mouse, in contrast to the decreased fat storage during pregnancy, we observed a much greater increase in adipose mass in MC3R KO versus WT mice (fig. S5). Thus, both deficient and excessive changes in adipose mass as a function of reproductive state may be observed in the MC3R KO.

DISCUSSION

Unlike mutations in leptin or melanocortin-4 signaling genes, MC3R deletion does not produce measurable hyperphagia or hypometabolism on normal chow, and the mild body composition phenotypes seen in these mice have been viewed as defective energy partitioning rather than defective energy homeostasis (*4*–*6*, *15*). However, MC3R KO animals do not exhibit normal homeostatic responses and, as shown here, exhibit excursions from energy set point in either direction when challenged with either internal or external nutritional stressors. Fasting reduces serum leptin and potently activates the AgRP neurons (*31*), yet the MC3R KO mouse exhibits defective behavioral (feeding), autonomic (EE), and neuroendocrine (HPT axis) responses to this strong orexigenic signal. While MC3R KO mice appear to defend set point and maintain constant body weight relatively well on normal chow, CR or high-fat chow produces greater weight loss or weight gain, respectively, compared to WT mice (Fig. 1E). Hence, the MC3R KO exhibits defective energy rheostasis; when animals are unperturbed, energy set point is relatively well maintained, but anorexigenic or orexigenic challenges highlight weak homeostatic boundary controls in these animals, resulting in excessive weight loss or weight gain.

α-MSH–induced GABA release has been demonstrated previously in a number of different brain regions but never in the context of MC3R regulation of MC4R mIPSC. An α-MSH–mediated increase in IPSCs in POMC neurons was shown previously and proposed to involve presynaptic MC3R, but POMC neurons do not express MC4R (*27*). Fu and van den Pol (*32*) showed that both MC4R and MC3R agonists increased IPSCs in neurons in the ventromedial nucleus of the hypothalamus (VMH), but the VMH cells were randomly selected and unlikely to be MC4R neurons, as they demonstrated no postsynaptic responses to α-MSH. Bagnol *et al.* (*9*) published the first paper showing that MC3R was coexpressed in POMC and AgRP neurons and hypothesized the existence of an MC3R-mediated inhibition of MC4R neuronal activity purely from anatomical principles. Thus, together, the data provided here finally prove a long-standing hypothesis: MC3R, functioning presynaptically on AgRP neurons, facilitates the release of GABA onto MC4R neurons to inhibit their activity. Since knockdown of MC3R mRNA in the ARC reproduces the defective refeeding and enhanced loss of weight in response to an energy deficit, this specific result is not a developmental consequence of MC3R loss and must involve primarily MC3R expressed in AgRP and POMC neurons of the ARC. The increased responsiveness to melanocortin administration fits well with a model (Fig. 2L) in which anorexigenic stimuli resulting from the activation of POMC neurons and release of α-MSH, followed by engagement of MC4R in sites such as the PVN, may ultimately be inhibited by α-MSH engagement of MC3R on AgRP termini, known to be found overlapping with POMC termini in many brain regions containing MC4R (*9*). Aside from one anatomical study showing that POMC boutons in the PVN exhibit both synaptic and nonsynaptic architecture and that POMC synpases in the PVN tend to be concentrated on distal dendrites while AgRP neuronal synapses tend to be concentrated on somata (*33*), we simply do not have enough anatomic or kinetic data to make many predictions regarding the spatial or temporal mechanisms by which α-MSH engages the MC4R and MC3R in regions such as the PVN. For example, while our electrophysiological data show that MC3R is acting presynaptically and MC4R postsynaptically in the PVN, we do not yet have ultrastructural data showing the precise subcellular localization of MC3R or MC4R proteins.

Previous research has shown that MC3R KO mice also exhibit a partial defect in activation of AgRP and NPY gene expression in the ARC in response to a fast, via an unknown mechanism (*15*, *17*), and this is likely to be a component of the defective responses to nutritional deficit shown here and reported previously (*15*, *17*). However, analysis of AgRP neuron-specific deletion of AgRP, NPY, or the vesicular GABA transporter Vgat shows that NPY and GABA can each independently mediate the acute feeding response to AgRP neuronal activation (*34*). Pharmacological blockade of either GABA or NPY in the PVN can inhibit feeding induced by optogenetic stimulation of AgRP axon terminals in the PVN (*35*). Further, GABA agonists alone, injected into the parabrachial nucleus, can rescue feeding in animals in which AgRP neurons have been ablated (*36*). Thus, the importance of GABA release by AgRP neurons in the control of food intake and energy homeostasis is indisputable, and it is likely that in the absence of the MC3R, the AgRP neurons have a general defect in fasting-induced activation that extends to the release of GABA as well. Further, the finding of a defective fasting-induced

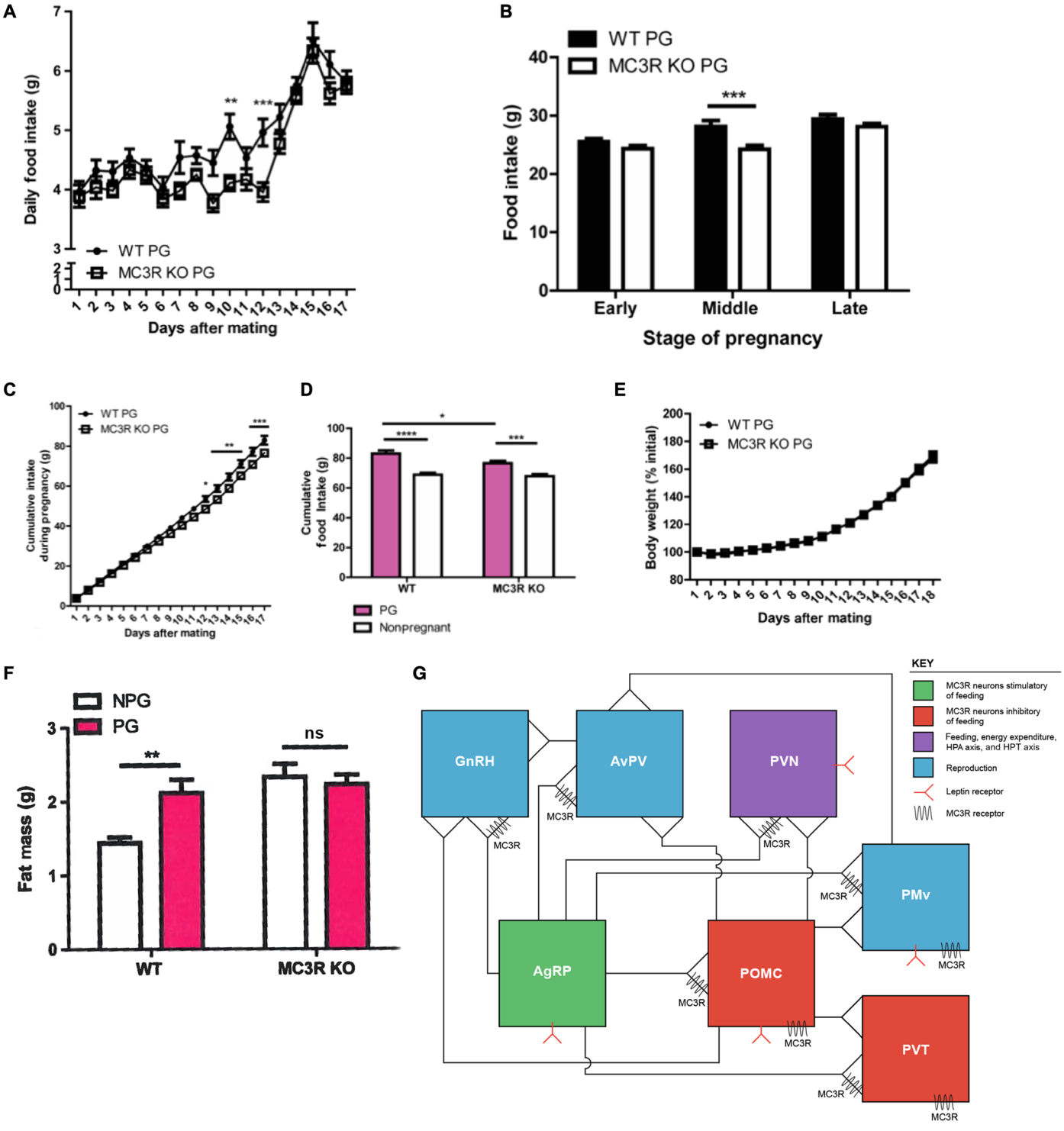

Fig. 4. Requirement for MC3R in reproductive rheostasis. (**A**) Daily food intake over the course of pregnancy (PG) in WT ($n = 19$) and MC3R KO mice ($n = 23$). (**B**) Analysis of cumulative food intake during the different stages of pregnancy in WT ($n = 19$) and MC3R KO mice ($n = 23$). (**C**) Cumulative food intake over the entire pregnancy in WT ($n = 19$) and MC3R KO mice ($n = 23$). (**D**) End point cumulative food intake comparison between WT nonpregnant ($n = 18$), WT pregnant ($n = 19$), MC3R KO nonpregnant ($n = 21$), and MC3R KO pregnant ($n = 23$) animals. (**E**) Body weight throughout pregnancy as a percent increase from baseline body weight in WT ($n = 19$) and MC3R KO ($n = 23$) pregnant dams. (**F**) Body composition analysis of fat mass in WT nonpregnant ($n = 11$), WT pregnant ($n = 7$), MC3RKO nonpregnant ($n = 12$), and MC3R KO pregnant ($n = 9$) animals. ns, not significant. (**G**) Diagram of the hypothalamic leptin-melanocortin system. MC3R is expressed in many AgRP projections and thus is likely to exert an inhibitory effect on MC4R target neurons involved in feeding, EE, neuroendocrine function, and reproductive functions. GnRH, gonadotropin-releasing hormone; AvPV, anteroventral periventricular nucleus; PMv, ventral premammilary nucleus. We performed statistical analyses (A to F) between WT and MC3R KO animals using two-way ANOVA with Bonferroni post hoc analysis. $^{***}P < 0.001$, $^{**}P < 0.01$, $^{*}P < 0.05$.

refeeding response following knockdown of MC3R just in the ARC (Fig. 1, K and L) also argues that this defect may be cell-autonomous; that is, loss of MC3R in AgRP neurons makes these cells less responsive to fasting-induced activation. The mechanism for this remains to be determined.

The role of MC3R in regulating GABA release from AgRP neurons argues for a molecular mechanism underlying control of lower homeostatic boundary conditions, in that activation of MC4R neurons by POMC-derived α-MSH undergoes MC3R-dependent inhibitory feedback. This may explain the increased and prolonged inhibition of feeding, the excessive EE seen in MC3R KO mice in models of melanocortin agonist administration (Fig. 3), and perhaps the enhanced cachexia reported in MC3R KO mice (*11*, *37*). MC3R in ARC is also required for normal rebound from a drop in energy stores, as in fasting or CR, and activation of MC3R neurons in ARC using DREADD (designer receptor exclusively activated by designer drug) technology produced profound hyperphagia and weight gain (fig. S6); however, the mechanisms here may be more complex, involving defects in up-regulation of AgRP and NPY gene expression along with defects in GABA release resulting from loss of the MC3R.

Mechanism(s) by which MC3R prevents excursion beyond upper homeostatic boundary conditions following high-fat feeding or ovariectomy remain to be tested. Two potential mechanisms could involve MC3R on either AgRP or POMC neurons. AgRP is a high-affinity MC3R antagonist, and thus, autofeedback inhibition of AgRP neurons via AgRP binding to MC3R on presynaptic terminals of these cells is possible. In addition, α-MSH released from POMC neurons might act in a feed-forward mechanism on presynaptic POMC MC3R sites to increase the activity of these anorexigenic neurons. However, it is important to remember that MC3R is expressed in many brain regions beyond the ARC, and again using DREADD technology, we show that activation of MC3R neurons in the paraventricular nucleus of the thalamus (PVT) inhibits food intake (fig. S6). Thus, the loss of MC3R from PVT neurons might remove an important anorexigenic input from outside the ARC. These data also argue that the bidirectional regulation of rheostasis by the MC3R is likely to involve MC3R neurons beyond the ARC (Fig. 4G).

MC3R KO animals show a significant deficit in cumulative food intake during the middle phase of pregnancy and a defect in total energy accretion during pregnancy compared with WT animals. MC3R KO animals also show a nondepot-specific accumulation of fat stores that is significantly greater than that observed in WT animals following ovariectomy, thus again highlighting energy stores that can diverge above or below normal levels, depending on the challenge. POMC and AgRP fiber densities show extensive overlap in many forebrain regions, including reproductive control centers, such as the ventral premammillary nucleus, anteroventral periventricular nucleus, and gonadotropin-releasing hormone neurons. Thus, it is expected that the MC3R-mediated regulatory feedback loop that we have identified for MC4R PVN neurons is functional in many other brain regions receiving POMC and AgRP projections.

Changes in reproductive state, such as pregnancy and menopause, involve the regulated movement from one energy set point to another, sometimes referred to as energy rheostasis in the agricultural literature (*30*), and these data further argue for a physiological role for MC3R in the regulation of rheostasis.

MATERIALS AND METHODS

Animal strains

MC3R KO, MC4R KO, and MC4R-GFP strains have been described previously (*2*, *5*, *26*) and maintained continuously by regular backcrossing onto C57BL/6J mice obtained from the Jackson Laboratory. MC3R-Cre mice are reported here for the first time. Mice containing bacterial artificial chromosome (BAC) DNA constructs expressing Cre recombinase under the control of the MC3R promoter were created in the Vanderbilt Transgenic Mouse Resource. Briefly, a DNA fragment containing a Cre recombinase sequence with kozak consensus and polyadenylation signal, followed by a FRT-flanked tetracycline resistance cassette from pFTet-129, was recombined at the ATG codon of the MC3R, using a 177-kb BAC cassette (BAC RP24-181G19) containing 125-kb 5′ and 50-kb 3′ to the single-coding exon *Mc3r* gene. The FLP (flippase recombinase) target (FLT) flanked Tet cassette was removed by FLP expression in bacteria, and the final BAC vector was shown to match predicted restriction digests by both a pulsed-field gel and standard "fingerprint" gel and by sequencing of all recombination junctions. Multiple transgenic lines were created and characterized by comparing the distribution of GFP immunoreactivity in the MC3R-GFP mouse with the distribution of TdTomato in MC3R-Cre tg/wt;TdTomato fl/wt. GFP distribution in MC3R-GFP mice was determined to represent bona fide sites of MC3R expression by dual in situ hybridization of MC3R mRNA and GFP mRNA using RNAscope. The MC3R-Cre mouse used in these studies exhibited matching distribution of immunoreactivity with the MC3R-GFP mouse in ARC, PVT, nucleus accumbens, and ventral tegmental area, all sites of known MC3R mRNA expression.

Food intake studies

All animal care and experimental procedures were approved by the Vanderbilt University Medical Center Institutional Animal Care and Use Committee or the University of Michigan Animal Care and Use Committee. WT male C57BL6/J mice were obtained from the Jackson Laboratory. Upon arrival, mice were single-housed and allowed to acclimatize at 22° to 24°C with a 12-hour light/12-hour dark cycle with standard chow and water provided ad libitum for 1 week. Unless otherwise described, all mice were fed a standard chow diet (S-5LOD, 13.5% kcal fat, 32.98% kcal protein, and 56.7% kcal carbohydrate; LabDiet). Diet-induced obesity was promoted by HFD (D12492, 60% kcal fat, 20% kcal protein, and 20% kcal carbohydrate; Research Diets). Food pellets were provided in a dish, and intake was measured manually, taking care to include all crumbs left in the dish.

CR experiments

MC3R KO, MC4R KO, and WT mice were individually caged starting at 8 weeks of age. Starting at 16 weeks of age, the food intake and body weight of the mice were monitored daily for 2 weeks. The average food consumed per mouse of each genotype was calculated, and this amount is referred to as the average food intake (AvFI). Next, mice were provided 70% of AvFI every day 1 hour before dark cycle (30% calorie restriction–30% CR).

Indirect calorimetry

Indirect calorimetry was performed by the Vanderbilt Mouse Metabolic Phenotyping Center (DK059637) using the Promethion system (Sable Systems International). Mice were individually housed at a standard 12-hour light/12-hour dark cycle. The Promethion system

allows continuous (at 5-min intervals) VO_2, VCO_2, physical activity, food intake, and body weight measurements. The body composition of the mice was measured before they were placed into the metabolic chambers and at the completion of the study. After 3 days of acclimation in the metabolic chambers, mice were fasted for 24 hours before receiving intraperitoneal injections of saline 30 min before the dark cycle. Mice were provided ad libitum access to chow at the beginning of the dark cycle. Three days after the first fast, mice were fasted for a second time for 24 hours and then received intraperitoneal injections of LY2112688 (10 mg/kg; #H-6268, Bachem) before the dark cycle. Food was provided at the beginning of the dark cycle. The average of 12 5-min measurement points collected per hour was used to calculate hourly EE.

TT4 measurements

Total serum T4 was measured in fasted and fed mice with enzyme-linked immunosorbent assay (ELISA; AccuDiag T4 ELISA Kit catalog #3149-18). Four to five drops of blood were collected by facial vein puncture and allowed to clot in microfuge tubes for 30 min at room temperature. Clot was removed by centrifugation (2000*g* for 10 min at 4°C), and serum was flash-frozen for further analysis according to the manufacturer's recommendations.

Preparation of lentiviral vectors

Mouse MC3R-specific shRNA clones in a pLKO.1 vector were purchased from Sigma-Aldrich. Scrambled shRNA in pLKO.1 was from Addgene (plasmid #1864). pLL3.7 was a gift from T. Nakagawa, Vanderbilt University and available at Addgene (plasmid #11795). An Xho I fragment of pLKO.1 containing the shRNA sequence was subcloned into a pLL3.7 vector digested with Xho I. HEK 293T cells were transfected with pLL3.7 (containing the shRNA for MC3R or scrambled shRNA), together with pRSV-REV, pVSVG, and pMDL. Forty-eight hours later, the supernatants were collected and filtered through a 0.45 μM filter. Lentiviral particles were precipitated by ultracentrifugation at 26,000 rpm at 4°C for 2 hours. The pellets were resuspended in 100 μl of phosphate-buffered saline (PBS). Viral titers were determined by the number of GFP-positive HEK 293T cells 48 hours after infection of cells with serial dilutions of the virus stocks.

DREADD viral injections

Stereotaxic viral injections of adeno-associated viral vectors (AAVs) expressing Cre recombinase–dependent expression of hM3Dq [AAV5-Ef1a-DIO-hM3D(Gq)-mCherry, Addgene) or mCherry (AAV5-Ef1a-DIO-mCherry, Addgene) were performed in adult MC3R-Cre mice (8 to 12 weeks old). Littermate mice were randomly assigned to experimental (DREADD-injected) or control groups (mCherry-injected) before viral injections. For viral injections, mice were anesthetized with isoflurene vapor and placed in a stereotaxic frame (Kopf). Small burr holes were made above either the arcuate nucleus or the PVT. A micromanipulator (Narishige) attached to a pulled micropipette (Drummond Scientific Company) was used to deliver viral vectors at a rate of 0.2 μl/min. A total of 30 to 50 nl of virus was injected unilaterally into either the arcuate nucleus [coordinates from bregma: anterior/posterior (A/P), −1.4; medial/lateral (M/L), 0.2; dorsal/ventral (D/V), −5.85 from brain surface] or the PVT (coordinates from bregma: A/P, −1/1; M/L, 0.0; D/V, −2.6 from brain surface). Injection needles were left in place for 10 min following viral injections to prevent leakage of virus. Three weeks were allowed following viral injections and before behavioral experiments to allow full viral expression.

Chemogenetic feeding assays

All chemogenetic feeding assays were performed on ad libitum fed mice during either the light period or the dark period of the light cycle. All mice were single-caged and handled daily for 1 week before feeding assays. Food intake was measured manually following intraperitoneal injections of sterile saline (0.9%, 200 μl) or clozapine N-oxide (CNO; 0.1 mg/kg, 200 μl; Enzo Life Sciences). Saline and CNO were administered randomly in a counterbalanced order, and average food intake following saline or CNO administration was calculated for each mouse for statistical analysis.

Immunohistochemistry and imaging

Cardiac perfusion was performed in all mice following chemogenetic experiments. Mice were perfused with 1× PBS, followed by 10% formalin. All brains were postfixed overnight in 10% formalin, followed by 20% sucrose in 1× PBS. Brain sections (30 μm) throughout the arcuate nucleus and PVT were prepared using a cryostat (Leica). Immunofluorescence imaging for mCherry was performed to confirm correct viral targeting in all mice injected with chemogenetic constructs. All mice without viral infection or viral infection targeted outside of ARC or PVT were excluded from analysis.

For cfos immunostaining, mice were injected with CNO (0.1 mg/kg ip, 200 μl) or sterile saline (0.9%, 200 μl) 30 min before perfusion. Brain sections were blocked for 1 hour in blocking buffer consisting of 2% bovine serum albumin (Sigma-Aldrich) in 1× PBS with 0.1% Tween 20. Sections were then incubated overnight in primary antibodies prepared in blocking buffer. Primary antibodies used included rabbit anti-cfos (1:5000; Calbiochem), goat anti-AgRP (1:200; R&D Systems), and chicken anti-GFP (1:1000; Abcam). Following primary antibody incubation, sections were washed three times for 10 min in 1× PBS, and secondary antibody prepared in blocking buffer was applied for 2 hours. Secondary antibodies included Alexa Fluor 594 donkey anti-rabbit, Alexa Fluor 647 donkey anti-goat, and Alexa Fluor 488 donkey anti-chicken (1:500; Thermo Fisher Scientific). Following incubation with secondary antibody, brain sections were washed with 1× PBS (3× washes for 10 min each) and mounted onto glass slides. To quantify cfos levels, cfos-positive cells were manually counted from sections containing viral infection in either arcuate nucleus or PVT. For each mouse in each experimental condition (saline or CNO), cfos was quantified from 5 to 10 sections, and an average number of cfos-positive cells was calculated for each mouse for statistical analysis.

Hypothalamic slice electrophysiology

MC4R-GFP mice were previously characterized by dual immunohistochemistry and in situ hybridization to validate the observation that GFP-positive neurons in the PVN expressed MC4R RNA. Male and female MC4R-GFP mice were deeply anesthetized with isoflurane before decapitation. The brain was entirely removed and immediately submerged in ice-cold, gassed (95% O_2 and 5% CO_2) artificial cerebrospinal fluid (aCSF), containing 126.2 mM NaCl, 3.1 mM KCl, 2 mM $CaCl_2$, 1 mM $MgCl_2$, 1 mM NaH_2PO_4, 26.2 mM $NaHCO_3$, 10 mM glucose, and 11 mM sucrose [320 mosmol/kg (pH 7.39) when gassed with 95% O_2 and 5% CO_2 at room temperature]. Coronal brain slices of 200-μm thickness were then cut and transferred to a glass beaker containing oxygenated aCSF at 31°C.

After an incubation period lasting at least 1 hour, a slice was transferred to a recording chamber (~2.0 ml in volume). To record from miniature EPSCs (mEPSCs), whole-cell recordings were performed using patch pipettes of 3.4- to 5-megohm resistance when filled with a solution containing 125 mM K gluconate, 8 mM KCl, 4 mM $MgCl_2$, 10 mM Hepes, 5 mM NaOH, 4 mM Na_2ATP, 0.4 mM Na_3GTP, 5 mM Na_2–creatine phosphate, 7 mM sucrose, and 7 mM KOH, which resulted in a pH ~7.23 and osmolality of 295 to 300 mosmol/kg. Recordings from mIPSCs were obtained using patch pipettes of 2.5- to 4-megohm resistance when filled with a solution containing 121 mM CsCl, 4 mM MgCl, 3 mM EGTA, 10 mM Hepes, 0.3 mM $CaCl_2$, 4 mM NaATP, 0.3 mM NaGTP, 14 mM creatinine phosphate (pH ~7.25) adjusted with CsOH, and osmolality of 295 to 300 mosmol/kg. Data were acquired at 10 kHz using a MultiClamp 700A amplifier (2000× gain; −3-dB filter frequency, 5 kHz) and Clampex 10.0.1 software (Axon Instruments). GraphPad Prism 6.0 (Graphpad Software Inc.) and Excel 2010 (Microsoft Corp.) were used for data analysis.

Deletion of AgRP neurons for slice recording

AgRP DTR mice, provided by R. Palmiter (*28*), were crossed to MC4R-GFP mice. The male offspring heterozygous for DTR and GFP of both sexes were then injected ip with DT (50 μg/kg) twice on the mornings of day 0 and day 2. Brain slices for electrophysiological analyses were prepared on the mornings of the days indicated in Fig. 2K. Body weight was monitored daily throughout the study.

Body composition

Whole-animal body composition analysis was performed using the Minispec Model mq7.5 (7.5 mHz; Bruker Instruments), which is a benchtop-pulsed 7-T NMR system. The instrument gives lean mass, fat mass, and fluid mass values. MC3R KO and WT female animals subjected to sham surgery or ovariectomy were analyzed at 14 to 16 weeks of age, and WT and MC3R KO pregnant and nonpregnant controls were analyzed at pregnancy day 18 or equivalent.

Melanocortin administration

Male mice of each genotype were divided into two subgroups, and each subgroup was given either vehicle (100 μl of saline) or LY2112688 (10.0 mg/kg) in 100 μl of saline ip half an hour before the beginning of the dark phase.

Food intake and body weight measurements during pregnancy

WT and MC3R KO females were paired with WT males overnight, and the presence of a vaginal plug was documented as pregnancy day 1. After verification of a vaginal plug, WT and MC3R KO dams were individually housed. Food intake and body weight were assessed daily.

Surgical ovariectomy

Female mice 8 to 9 weeks in age were subjected to ovariectomy as previously described (*38*). Briefly, mice were laid on their ventral surface with their tail toward the surgeon. A small midline incision was made on the dorsal surface midway between the base of the tail and the middle of the back. In a point lateral to the paraspinous muscles, the peritoneal cavity was punctured, and the ovary was then pulled through the incision by grasping the periovarian fat pad. A hemostat was clamped around the uterine vasculature between the oviduct and uterus. The ovary and a small part of the oviduct were then removed with a single cut. The hemostat was then removed, and the remaining tissue was reinserted into the peritoneal cavity via the entrance incision. The ovary on the contralateral side was then removed in a similar matter. The skin incision was sealed with Vetbond, and the animals were returned to warm cages for postoperative care. Four to six weeks after surgery, animals were euthanized, and tissue was collected for analysis.

Statistical analyses

All statistical analyses were performed using GraphPad Prism. The number of samples and the statistical tests used in each experiment are described in the figure legends.

SUPPLEMENTARY MATERIALS

Supplementary material for this article is available at http://advances.sciencemag.org/cgi/content/full/4/8/eaat0866/DC1

Fig. S1. Validation of a lentiviral shMC3R vector and viral injections.
Fig. S2. α-MSH fails to modulate the frequency or amplitude of TTX-resistant mEPSCs in MC4R PVN neurons.
Fig. S3. Neither endocannabinoids nor nitric oxide mediates the α-MSH–induced increase in mIPSC frequency.
Fig. S4. Reduction of AgRP cell numbers following DT treatment of AgRP-DTR mice.
Fig. S5. Body weight and fat mass changes in response to ovariectomy.
Fig. S6. Bidirectional regulation of feeding by MC3R neurons.

REFERENCES AND NOTES

1. W. Fan, B. A. Boston, R. A. Kesterson, V. J. Hruby, R. D. Cone, Role of melanocortinergic neurons in feeding and the *agouti* obesity syndrome. *Nature* **385**, 165–168 (1997).
2. D. Huszar, C. A. Lynch, V. Fairchild-Huntress, J. H. Dunmore, Q. Fang, L. R. Berkemeier, W. Gu, R. A. Kesterson, B. A. Boston, R. D. Cone, F. J. Smith, L. A. Campfield, P. Burn, F. Lee, Targeted disruption of the melanocortin-4 receptor results in obesity in mice. *Cell* **88**, 131–141 (1997).
3. I. S. Farooqi, J. M. Keogh, G. S. Yeo, E. J. Lank, T. Cheetham, S. O'Rahilly, Clinical spectrum of obesity and mutations in the melanocortin 4 receptor gene. *N. Engl. J. Med.* **348**, 1085–1095 (2003).
4. A. S. Chen, D. J. Marsh, M. E. Trumbauer, E. G. Frazier, X.-M. Guan, H. Yu, C. I. Rosenblum, A. Vongs, Y. Feng, L. Cao, J. M. Metzger, A. M. Strack, R. E. Camacho, T. N. Mellin, C. N. Nunes, W. Min, J. Fisher, S. Gopal-Truter, D. E. MacIntyre, H. Y. Chen, L. H. Van der Ploeg, Inactivation of the mouse melanocortin-3 receptor results in increased fat mass and reduced lean body mass. *Nat. Genet.* **26**, 97–102 (2000).
5. A. A. Butler, R. A. Kesteson, K. Khong, M. Jane Cullen, M. A. Pelleymounter, J. Dekoning, M. Baetscher, R. D. Cone, A unique metabolic syndrome causes obesity in the melanocortin-3 receptor-deficient mouse. *Endocrinology* **141**, 3518–3521 (2000).
6. P. You, H. Hu, Y. Chen, Y. Zhao, Y. Yang, T. Wang, R. Xing, Y. Shao, W. Zhang, D. Li, H. Chen, M. Liu, Effects of melanocortin 3 and 4 receptor deficiency on energy homeostasis in rats. *Sci. Rep.* **6**, 34938 (2016).
7. I. Gantz, Y. Konda, T. Tashiro, Y. Shimoto, H. Miwa, G. Munzert, S. J. Watson, J. DelValle, T. Yamada, Molecular cloning of a novel melanocortin receptor. *J. Biol. Chem.* **268**, 8246–8250 (1993).
8. L. Roselli-Rehfuss, K. G. Mountjoy, L. S. Robbins, M. T. Mortrud, M. J. Low, J. B. Tatro, M. L. Entwistle, R. B. Simerly, R. D. Cone, Identification of a receptor for gamma melanotropin and other proopiomelanocortin peptides in the hypothalamus and limbic system. *Proc. Natl. Acad. Sci. U.S.A.* **90**, 8856–8860 (1993).
9. D. Bagnol, X.-Y. Lu, C. B. Kaelin, H. E. W. Day, M. Ollmann, I. Gantz, H. Akil, G. S. Barsh, S. J. Watson, The anatomy of an endogenous antagonist: Relationship between agouti- related protein and proopiomelanocortin in brain. *J. Neurosci.* **19**, RC26 (1999).
10. C. Haskell-Luevano, P. Chen, C. Li, K. Chang, M. S. Smith, J. L. Cameron, R. D. Cone, Characterization of the neuroanatomical distribution of agouti-related protein immunoreactivity in the rhesus monkey and the rat. *Endocrinology* **140**, 1408–1415 (1999).
11. D. L. Marks, R. D. Cone, Central melanocortins and the regulation of weight during acute and chronic disease. *Recent Prog. Horm. Res.* **56**, 359–375 (2001).
12. D. L. Marks, A. A. Butler, R. Turner, G. Brookhart, R. D. Cone, Differential role of melanocortin receptor subtypes in cachexia. *Endocrinology* **144**, 1513–1523 (2003).
13. W. Cheung, P. X. Yu, B. M. Little, R. D. Cone, D. L. Marks, R. H. Mak, Role of leptin and melanocortin signaling in uremia-associated cachexia. *J. Clin. Invest.* **115**, 1659–1665 (2005).

14. J. M. Scarlett, D. D. Bowe, X. Zhu, A. K. Batra, W. F. Grant, D. L. Marks, Genetic and pharmacologic blockade of central melanocortin signaling attenuates cardiac cachexia in rodent models of heart failure. *J. Endocrinol.* **206**, 121–130 (2010).
15. B. J. Renquist, J. G. Murphy, E. A. Larson, D. Olsen, R. F. Klein, K. L. J. Ellacott, R. D. Cone, Melanocortin-3 receptor regulates the normal fasting response. *Proc. Natl. Acad. Sci. U.S.A.* **109**, E1489–E1498 (2012).
16. G. M. Sutton, D. Perez-Tilve, R. Nogueiras, J. Fang, J. K. Kim, R. D. Cone, J. M. Gimble, M. H. Tschöp, A. A. Butler, The melanocortin-3 receptor is required for entrainment to meal intake. *J. Neurosci.* **28**, 12946–12955 (2008).
17. C. Girardet, M. M. Mavrikaki, J. R. Stevens, C. A. Miller, D. L. Marks, A. A. Butler, Melanocortin-3 receptors expressed in Nkx2.1(+ve) neurons are sufficient for controlling appetitive responses to hypocaloric conditioning. *Sci. Rep.* **7**, 44444 (2017).
18. D. L. Marks, V. Hruby, G. Brookhart, R. D. Cone, The regulation of food intake by selective stimulation of the type 3 melanocortin receptor (MC3R). *Peptides* **27**, 259–264 (2006).
19. M. Lee, A. Kim, I. M. Conwell, V. Hruby, A. Mayorov, M. Cai, S. L. Wardlaw, Effects of selective modulation of the central melanocortin-3-receptor on food intake and hypothalamic POMC expression. *Peptides* **29**, 440–447 (2008).
20. N. Balthasar, L. T. Dalgaard, C. E. Lee, J. Yu, H. Funahashi, T. Williams, M. Ferreira, V. Tang, R. A. McGovern, C. D. Kenny, L. M. Christiansen, E. Edelstein, B. Choi, O. Boss, C. Aschkenasi, C. Y. Zhang, K. Mountjoy, T. Kishi, J. K. Elmquist, B. B. Lowell, Divergence of melanocortin pathways in the control of food intake and energy expenditure. *Cell* **123**, 493–505 (2005).
21. A. Boelen, W. M. Wiersinga, E. Fliers, Fasting-induced changes in the hypothalamus-pituitary–thyroid axis. *Thyroid* **18**, 123–129 (2008).
22. M. Harris, C. Aschkenasi, C. F. Elias, A. Chandrankunnel, E. A. Nillni, C. Bjørbæk, J. K. Elmquist, J. S. Flier, A. N. Hollenberg, Transcriptional regulation of the thyrotropin-releasing hormone gene by leptin and melanocortin signaling. *J. Clin. Invest.* **107**, 111–120 (2001).
23. M. Ghamari-Langroudi, Electrophysiological analysis of circuits controlling energy homeostasis. *Mol. Neurobiol.* **45**, 258–278 (2012).
24. M. Ghamari-Langroudi, K. R. Vella, D. Srisai, M. L. Sugrue, A. N. Hollenberg, R. D. Cone, Regulation of thyrotropin-releasing hormone-expressing neurons in paraventricular nucleus of the hypothalamus by signals of adiposity. *Mol. Endocrinol.* **24**, 2366–2381 (2010).
25. M. Ghamari-Langroudi, G. J. Digby, J. A. Sebag, G. L. Millhauser, R. Palomino, R. Matthews, T. Gillyard, B. L. Panaro, I. R. Tough, H. M. Cox, J. S. Denton, R. D. Cone, G-protein-independent coupling of MC4R to Kir7.1 in hypothalamic neurons. *Nature* **520**, 94–98 (2015).
26. H. Liu, T. Kishi, A. G. Roseberry, X. Cai, C. E. Lee, J. M. Montez, J. M. Friedman, J. K. Elmquist, Transgenic mice expressing green fluorescent protein under the control of the melanocortin-4 receptor promoter. *J. Neurosci.* **23**, 7143–7154 (2003).
27. M. A. Cowley, J. L. Smart, M. Rubinstein, M. G. Cerdán, S. Diano, T. L. Horvath, R. D. Cone, M. J. Low, Leptin activates anorexigenic POMC neurons through a neural network in the arcuate nucleus. *Nature* **411**, 480–484 (2001).
28. S. Luquet, F. A. Perez, T. S. Hnasko, R. D. Palmiter, NPY/AgRP neurons are essential for feeding in adult mice but can be ablated in neonates. *Science* **310**, 683–685 (2005).
29. B. M. Molden, K. A. Cooney, K. West, L. H. Van Der Ploeg, G. Baldini, Temporal cAMP signaling selectivity by natural and synthetic MC4R agonists. *Mol. Endocrinol.* **29**, 1619–1633 (2015).
30. N. Mrosovsky, *Rheostasis, the Physiology of Change*. (Oxford Univ. Press, 1990).
31. K. A. Takahashi, R. D. Cone, Fasting induces a large, leptin-dependent increase in the intrinsic action potential frequency of orexigenic arcuate nucleus neuropeptide Y/Agouti-related protein neurons. *Endocrinology* **146**, 1043–1047 (2005).
32. L. Y. Fu, A. N. van den Pol, Agouti-related peptide and MC3/4 receptor agonists both inhibit excitatory hypothalamic ventromedial nucleus neurons. *J. Neurosci.* **28**, 5433–5449 (2008).
33. D. Atasoy, J. N. Betley, W.-P. Li, H. H. Su, S. M. Sertel, L. K. Scheffer, J. H. Simpson, R. D. Fetter, S. M. Sternson, A genetically specified connectomics approach applied to long-range feeding regulatory circuits. *Nat. Neurosci.* **17**, 1830–1839 (2014).
34. M. J. Krashes, B. P. Shah, S. Koda, B. B. Lowell, Rapid versus delayed stimulation of feeding by the endogenously released AgRP neuron mediators GABA, NPY, and AgRP. *Cell Metab.* **18**, 588–595 (2013).
35. D. Atasoy, J. N. Betley, H. H. Su, S. M. Sternson, Deconstruction of a neural circuit for hunger. *Nature* **488**, 172–177 (2012).
36. Q. Wu, R. D. Palmiter, GABAergic signaling by AgRP neurons prevents anorexia via a melanocortin-independent mechanism. *Eur. J. Pharmacol.* **660**, 21–27 (2011).
37. D. L. Marks, R. D. Cone, The role of the melanocortin-3 receptor in cachexia. *Ann. N. Y. Acad. Sci.* **994**, 258–266 (2003).
38. M. N. Martinez, C. H. Emfinger, M. Overton, S. Hill, T. S. Ramaswamy, D. A. Cappel, K. Wu, S. Fazio, W. H. McDonald, D. L. Hachey, D. L. Tabb, J. M. Stafford, Obesity and altered glucose metabolism impact HDL composition in CETP transgenic mice: A role for ovarian hormones. *J. Lipid Res.* **53**, 379–389 (2012).

Acknowledgments: We would like to thank S. Y. Williams and H. Adams for excellent technical assistance with these experiments and T. Gillyard and S. King for their excellent contributions to the creation of figures and illustrations. **Funding:** This was supported by NIH grant DK070332 (R.D.C. and M.G.-L.) and F30 DK108476-01 (M.J.L.). **Author contributions:** M.G.-L., I.C., R.N.L., P.S., M.J.L., and K.L.J.E. performed experiments, analyzed data, prepared figures, and assisted with editing of the manuscript. M.G.-L. and R.D.C. wrote the manuscript. R.D.C. analyzed data, prepared figures, and provided the oversight for the experimental work and statistical analysis. **Competing interests:** The authors declare that they have no competing interests. **Data and materials availability:** All data needed to evaluate the conclusions are provided in the paper and/or the Supplementary Materials. Additional data related to this paper may be requested from the authors. All mouse strains are available from the Jackson Laboratory or directly from the authors (MC3R-Cre).

Submitted 22 January 2018
Accepted 18 July 2018
Published 22 August 2018
10.1126/sciadv.aat0866

Citation: M. Ghamari-Langroudi, I. Cakir, R. N. Lippert, P. Sweeney, M. J. Litt, K. L. J. Ellacott, R. D. Cone, Regulation of energy rheostasis by the melanocortin-3 receptor. *Sci. Adv.* **4**, eaat0866 (2018).

ScienceAdvances

Regulation of energy rheostasis by the melanocortin-3 receptor

Masoud Ghamari-Langroudi, Isin Cakir, Rachel N. Lippert, Patrick Sweeney, Michael J. Litt, Kate L. J. Ellacott and Roger D. Cone

Sci Adv **4** (8), eaat0866.
DOI: 10.1126/sciadv.aat0866

Science Advances
AAAS

advances.sciencemag.org/cgi/content/full/4/8/eaat0866/DC1

Supplementary Materials for

Regulation of energy rheostasis by the melanocortin-3 receptor

Masoud Ghamari-Langroudi*, Isin Cakir, Rachel N. Lippert, Patrick Sweeney, Michael J. Litt, Kate L. J. Ellacott, Roger D. Cone*

*Corresponding author. Email: masoud.ghamari-langroudi@vanderbilt.edu (M.G.-L.); rcone@umich.edu (R.D.C.)

Published 22 August 2018, *Sci. Adv.* **4**, eaat0866 (2018)
DOI: 10.1126/sciadv.aat0866

This PDF file includes:

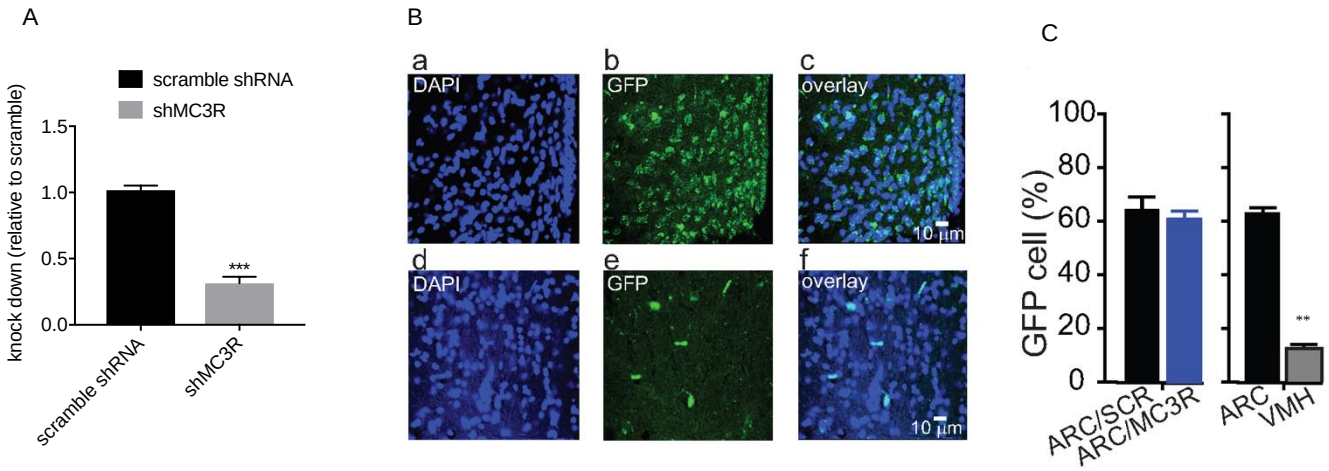

Fig. S1. Validation of a lentiviral shMC3R vector and viral injections. (**A**) Lentiviral vectors were validated using HEK 293 cells transfected with an mMC3R expression vector. mMC3R mRNA expression was measured in cells infected with shMC3R and a control scrambled shRNA virus by qRTPCR, and normalized to β-actin mRNA levels. Data show the mean and SEM for 3 infections (unpaired t-test, ***$p<0.001$). (**B** to **C**) *post hoc* analysis of injection sites and transduction efficacy of viral particles in mice after completion of the experiments shown in Fig. 1K-M. DAPi stained (a&d), GFP expressing (b&e), and co-stained (c&f) neurons in the hypothalamic sections from ARC (a-c) and VMH (d-f) of these mice were counted. Cells that stained with DAPi and expressed GFP were considered neurons transduced with a lentiviral particle. Our analysis indicates that the ratio of GFP expressing neurons in the ARC that stained with DAPi was not different in MC3R shRNA expressing than scramble expressing mice ($p>0.05$, unpaired t-test). The average of transduction efficiency counted in all ARC sections (62+/- 2%) was significantly greater than more dorsal areas of hypothalamus nor receiving injection, such as VMH (12+/- 1%, **$p<0.05$, unpaired t-test).

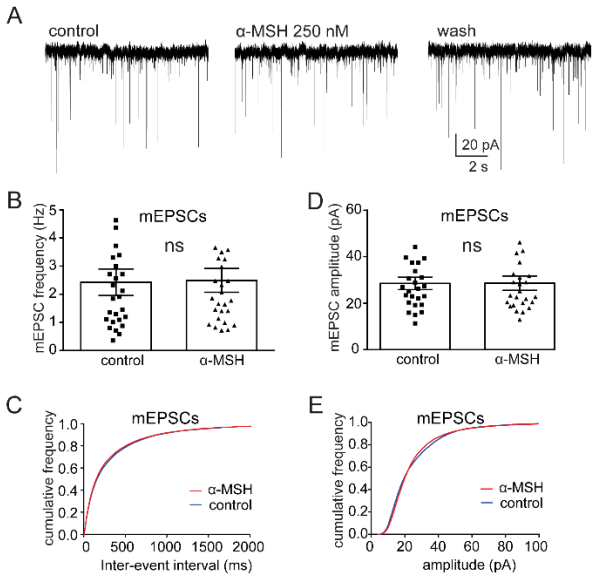

Fig. S2. α-MSH fails to modulate the frequency or amplitude of TTX-resistant mEPSCs in MC4R PVN neurons. (**A**) Panels are representative current traces of a recording from a MC4R PVN neuron voltage clamped at -70 mV by using K+ Gluconate filled patch electrodes in the presence of 0.5 μM TTX and 200 μM picrotoxin to block Na+ dependent action potentials, and GABA(A) receptors, respectively. (**B**) The bar graphs represent the mean +/-SEM of the frequency of mEPSCs in control and in 250 nM α-MSH. The peptide failed to significantly affect the frequency of mEPSCs (from 2.43+/-0.47 Hz in control to 2.49 +/-0.42 Hz in peptide, ns indicates p>0.5 by paired t-test, n=26). (**C**) The cumulative frequency distribution of mEPSCs recorded in control and in α-MSH are not significantly different (p>0.05, by Kolmogorov-Smirnov test). (**D** to **E**) The bar graphs represent the mean +/-SEM of the amplitudes of mEPSCs in control and in 250 nM α-MSH. The peptide has no significant effects on the mean or cumulative frequency distributions of the amplitude of mEPSCs when compared to control condition (D: from 28.5 +/-2.6 pA in control to 28.6 +/-3.1 pA in the peptide, ns indicates p>0.05 by paired t-test, n=25, E: p>0.05, by Kolmogorov-Smirnov test).

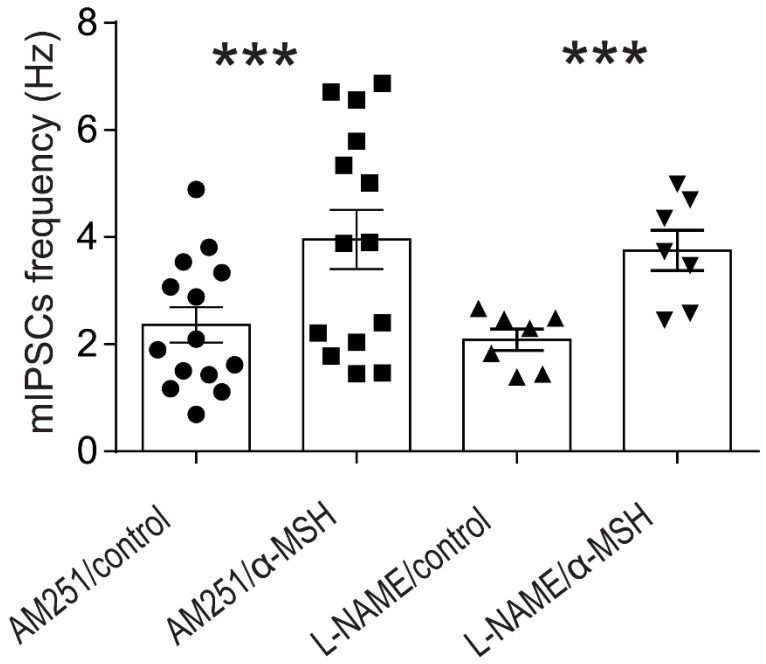

Fig. S3. Neither endocannabinoids nor nitric oxide mediates the α-MSH–induced increase in mIPSC frequency. The bar graph represents the mean +/-SEM of the frequency of mIPSCs recorded from PVN MC4R neurons pretreated more than one hour with 10 μM AM251 or 100 μM L-NAME before and after applications of 250 nM α-MSH. Pretreatment of neurons with 10 μM AM251 fails to block the α-MSH -induced increase in the frequency of mIPSCs (from 2.36 +/-0.33 Hz in control to 4.0 +/- 0.6 Hz in AM251, *** indicate $p < 0.0005$, paired t-test, n=15). 100 μM L-NAME also fails to block the α-MSH –induced increase in mIPSCs (from 2.18 +/- 0.2 Hz in control to 3.9+/- 0.4 Hz in L-NAME, *** indicates $p < 0.0005$, paired t-test, n=8).

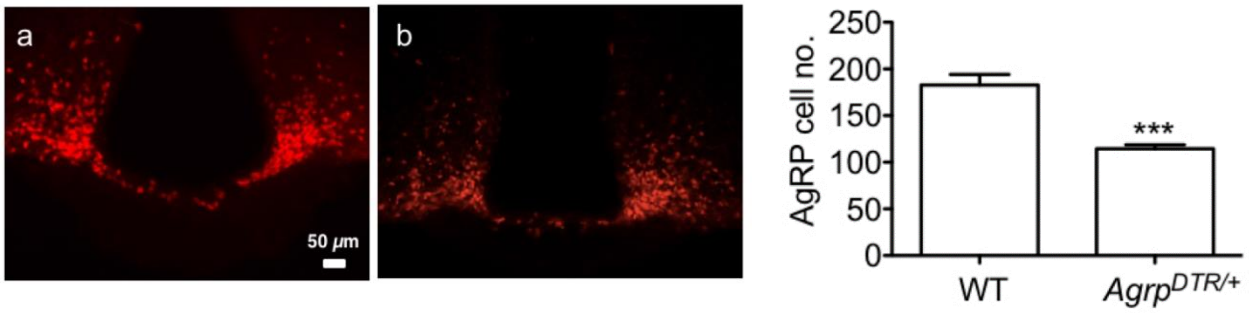

Fig. S4. Reduction of AgRP cell numbers following DT treatment of AgRP-DTR mice. AgRP neuron counts before (**a**) and 6 days after (**b**) DT injections into AgRP-DTR mice. The bar graph represents the mean +/-SEM of the frequency of neurons counted in 19 (WT) and 48 (MC3R KO) sections from 4 mice per group, p value< 0.0001, unpaired t-test.

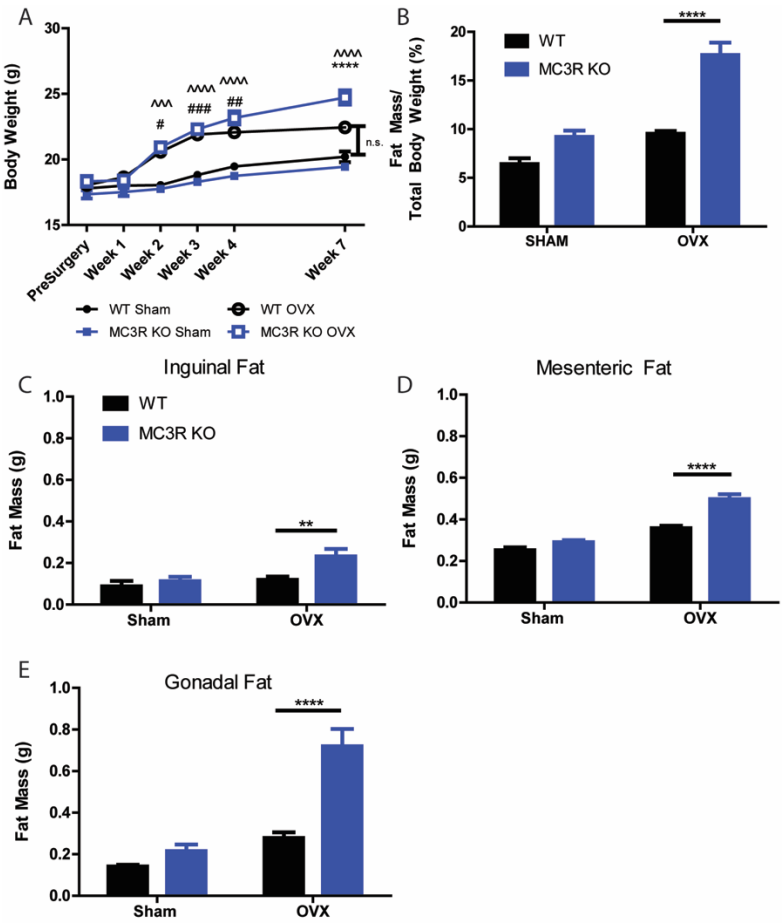

Fig. S5. Body weight and fat mass changes in response to ovariectomy. (**A**) Body weight gain in WT Sham (closed black circles, n=4), MC3R KO Sham (closed blue squares, n=5), WT OVX (open black circles, n=18) and MC3R KO OVX (open blue squares, n=14). (**B**) Body fat mass percentage in WT Sham (n=4), MC3R KO Sham (n=5), WT OVX (n=18) and MC3R KO OVX (n=14) at 14-16 weeks old. (**C**) Inguinal, (**D**) mesenteric and (**E**) gonadal fat pads weight in MC3R KO OVX (n=14), MC3R KO Sham (n=5), WT Sham (n=4) and WT OVX (n=17) animals. Statistics were performed using Two Way ANOVA with a Bonferroni post-test for comparison between groups. (^, ^^^,^^^^ $p<0.05$, $p<0.001$, $p<0.0001$ MC3R KO OVX vs. MC3R KO Sham, respectively, #,##,###, $p<0.05$, $p<0.01$, $p<0.001$ WT OVX vs. WT Sham, respectively, **,****, $p<0.01$, $p<0.0001$ MC3R KO OVX vs. WT OVX).

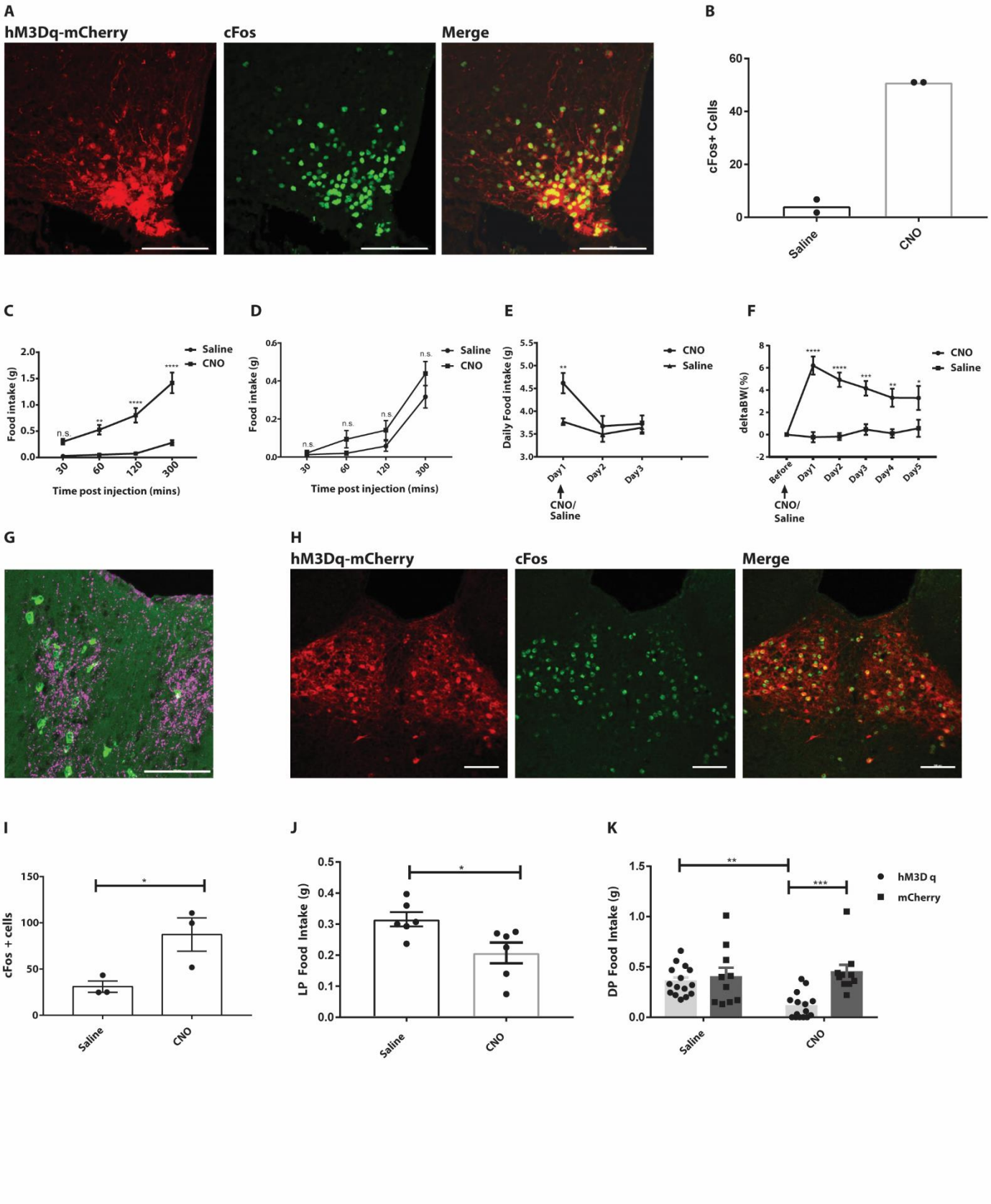
A
hM3Dq-mCherry
cFos
Merge
B
cFos+ Cells
Saline
CNO
C
Food intake (g)
Saline
CNO
n.s.
**
****
Time post injection (mins)
D
Food intake (g)
Saline
CNO
n.s.
Time post injection (mins)
E
Daily Food intake (g)
CNO
Saline
**
Day1
Day2
Day3
CNO/
Saline
F
deltaBW(%)
CNO
Saline
****
***
**
*
Before
Day1
Day2
Day3
Day4
Day5
CNO/
Saline
G
H
hM3Dq-mCherry
cFos
Merge
I
cFos + cells
*
Saline
CNO
J
LP Food Intake (g)
*
Saline
CNO
K
DP Food Intake (g)
**
***
hM3D q
mCherry
Saline
CNO

Fig. 1

Fig. S6. Bidirectional regulation of feeding by MC3R neurons. (A) DREADD induced activation of arcuate MC3R expressing neurons. Representative images showing hM3Dq-mCherry (left panel), cfos (middle panel), and a merged image (right panel) in a mouse transfected with hM3Dq in arcuate MC3R expressing neurons following CNO administration. **(B)** Quantification of cfos expression in the arcuate nucleus following i.p. injections of saline or CNO. CNO injections increased cfos expression in the arcuate nucleus. **(C)** Acute feeding assays following DREADD mediated activation of arcuate MC3R neurons. Activation of MC3R neurons increased food intake at all times tested (Two-Way ANOVA with Bonferroni post-hoc test, n=10 mice). **(D)** Acute feeding assays in control mice with viral infections outside of the arcuate nucleus. Administration of CNO did not affect food intake at any time point tested (Two-Way ANOVA with Bonferroni post-hoc test, n=8 mice). **(E)** Daily 24hr food intake following a single i.p. injection of CNO. CNO increased food intake 24hr post injection with food intake returning to basal levels on the second and third day post injection (Two-Way ANOVA with Bonferroni post-hoc test, n=10 mice). **(F)** Change in body weight following a single injection of CNO or saline. Body weight increased on the day following CNO injection, remaining elevated five days following CNO injection (Two-Way ANOVA with Bonferroni post-hoc test, n=10 mice). **(G)** MC3R expression in the paraventricular thalamus (PVT) of a MC3R-Cre, L10aGFP reporter mouse (green) with overlapping AgRP projection fibers (purple). **(H)** DREADD induced activation of PVT MC3R neurons. Representative images showing hM3Dq-mCherry (left panel), cfos (middle panel), and a merged image (right panel) following an i.p. injection of CNO. **(I)** Quantification of cfos expression in the PVT following i.p. injections of saline or CNO (unpaired Student's t-test, n=3 mice per group). **(J)** Light period food intake following i.p. injections of saline or CNO. CNO injections reduced food intake during the light period (paired Student's t-test, n=6 mice). **(K)** Dark period food intake assays. CNO injections reduced food intake in mice transduced with hM3Dq in PVT MC3R neurons, but not in mice transduced with control mCherry expressing virus in PVT MC3R neurons (Two-Way ANOVA with Bonferroni post-hoc test, n=14 mice for hM3Dq group and n=8 mice for mCherry group). CNO was injected at a dose of 0.1mg/kg (200ul) for all experiments. LP (light period), DP (dark period), CNO (clozapine-N-oxide). A, G, &H: Scale bars, 100 μm.